1-1-2013

In vivo Dark-field Imaging of the Retinal Pigment Epithelium Cell Mosaic

Drew Scoles
University of Rochester

Yusufu N. Sulai
University of Rochester

Alfredo Dubra
Marquette University

Accepted version. *Biomedical Optics Express*, Vol. 4, No. 9 (2013): 1710-1723. DOI.

In vivo Dark-Field Imaging of the Retinal Pigment Epithelium Cell Mosaic

Drew Scoles
Department of Biomedical Engineering, University of Rochester
Rochester, NY
Yusufu N. Sulai
The Institute of Optics, University of Rochester
Rochester, NY
Alfredo Dubra
Department of Ophthalmology, Medical College of Wisconsin
Department of Biophysics, Medical College of Wisconsin
Department of Biomedical Engineering, Marquette University
Milwaukee, WI

Abstract

Non-invasive reflectance imaging of the human RPE cell mosaic is demonstrated using a modified confocal adaptive optics scanning light ophthalmoscope (AOSLO). The confocal circular aperture in front of the imaging detector was replaced with a combination of a circular aperture 4 to 16 Airy disks in diameter and an opaque filament, 1 or 3 Airy disks thick. This arrangement reveals the RPE cell mosaic by dramatically attenuating the light backscattered by the photoreceptors. The RPE cell mosaic was visualized in all 7 recruited subjects at multiple retinal locations with varying degrees of contrast and cross-talk from the photoreceptors. Various experimental settings were explored for improving the visualization of the RPE cell

[Citation: Journal/Monograph Title, Vol. XX, No. X (yyyy): pg. XX-XX. DOI.

boundaries including: pinhole diameter, filament thickness, illumination and imaging pupil apodization, unmatched imaging and illumination focus, wavelength and polarization. None of these offered an obvious path for enhancing image contrast. The demonstrated implementation of dark-field AOSLO imaging using 790 nm light requires low light exposures relative to light safety standards and it is more comfortable for the subject than the traditional autofluorescence RPE imaging with visible light. Both these factors make RPE dark-field imaging appealing for studying mechanisms of eye disease, as well as a clinical tool for screening and monitoring disease progression.

OCIS codes: (170.4460) Ophthalmic optics and devices, (170.4470) Ophthalmology, (290.4210) Multiple scattering, (110.1080) Active or adaptive optics

1. Introduction

The retinal pigment epithelium (RPE) lies directly posterior to the photoreceptor layer, with apical processes enveloping the outer segments of rods and cones [1]. This proximity allows the RPE to phagocytize the photoreceptor outer segments, and assist in the turnover of visual pigments [2]. This homeostatic role of the RPE is essential to normal health [3], and diseased RPE has been implicated in the pathogenesis of age-related macular degeneration [4], diabetic retinopathy [5], Stargardt's disease [6], Best's disease [7], Leber's congenital amaurosis [8] and retinitis pigmentosa [9].

Currently, in order to evaluate the health of the RPE *in vivo*, the autofluorescence of the fundus is imaged using visible or near-infrared light, with hyper, or hypo-fluorescence revealing areas of disease and/or cell loss [10–12]. In addition, spectral domain optical coherence tomographs (SD-OCTs) can resolve two highly reflective layers believed to contain contributions from RPE cells [13]. Breaks in these reflective layers are typically interpreted as areas of RPE loss [14]. Recent work suggests, however, that individual RPE cell loss and dysmorphology are early biomarkers of disease [4]. Neither conventional wide-field fundus autofluorescence nor SD-OCT can evaluate structural changes at the cellular scale, and hence the need for higher spatial resolution imaging techniques. The use of adaptive optics scanning light ophthalmoscopes (AOSLOs), has allowed *in vivo* imaging of individual RPE cells in non-human primates and human

volunteers using the intrinsic fluorescence of the lipofuscin, allowing for analyses previously possible only with histology [15,16]. Despite this advance, the use of AOSLO for imaging RPE has remained limited both due to light safety concerns [17–20] and subject discomfort. Confocal reflectance AOSLO imaging has also revealed the RPE mosaic using near infrared light, in conditions where the photoreceptors are diseased or displaced from the RPE due to fluid [21].

The motivation for this work was to develop a method for visualizing the RPE cell mosaic non-invasively with better light safety than that of autofluorescence imaging. In what follows, we show experimental evidence that this can be achieved in subjects with normal retinal architecture with moderate success, using near-infrared light in a modified AOSLO. The AOSLO was converted for RPE imaging by replacing the confocal aperture with a spatial filter inspired by the work of Webb *et al.* [22][REMOVED HYPERLINK FIELD] and others [23–26]. The proposed spatial filter blocks the confocal signal, preferentially attenuating light back-scattered by the photoreceptors, while passing the light multiply-scattered by the RPE cells, thus revealing their structure. Various imaging parameters including: pinhole diameter, filter thickness, illumination and imaging pupil apodization, unmatched imaging and illumination focus, wavelength and polarization, were varied in order to improve the visualization of the RPE cell boundaries. This dark-field imaging technique [27] is validated against AOSLO autofluorescence in a subject free from eye disease, as well as confocal AOSLO reflectance in a subject with central serous retinopathy.

2. Methods

2.1 Human Subjects

Research procedures followed the tenets of the Declaration of Helsinki and informed written consent was obtained from all subjects. The study protocol was approved by the institutional review board of the Medical College of Wisconsin. Seven normal volunteers were recruited for the study, aged 19-40 years. One 65 years old subject (DW_1188) diagnosed with central serous retinopathy was recruited for validation of the dark-field visualization of the RPE mosaic. Axial

length measurements were obtained on all subjects (Zeiss IOL Master; Carl Zeiss Meditec, Dublin, CA, USA) in order to determine the scale (in microns per pixel) of each retinal image. Prior to retinal imaging, the eye was dilated and cycloplegia was induced through topical application of phenylephrine hydrochloride (2.5%) and tropicamide (1%).

2.2 Spectral-Domain Optical Coherence Tomography

SD-OCT volumetric and line scan images were acquired (Bioptigen, Research Triangle Park, NC, USA) at regions of planned AO imaging and averaged as previously described [28]. A 3×3 mm macular volume scan was manually registered and used to create an *en face* view of the choroid of subject AD_1025.

2.3 AOSLO reflectance imaging

A custom AOSLO [29] was used for this study. The detection path was modified by replacing the confocal aperture (Fig. 1(a)) in the image plane in front of the detector, with a larger aperture and a centered filament. Pinholes with 4, 8, 12 and 16 Airy disk diameters (ADD) and filaments 1 and 3 ADD thick were evaluated to enhance RPE signal relative to that of the photoreceptors. The filament was always aligned to maximally block the directly back-scattered light (confocal signal) from a model eye. This is a dark-field configuration [27], in which we believe the source of image contrast is multiple scattering. To further explore the attenuation of photoreceptor signal, we tested apodizing masks with annular binary transmission in the pupil of the illumination and/or imaging paths [30] in subject JC_0616 to take advantage of the Stiles-Crawford effect [31]. Three additional experiments were performed in an attempt to improve the resolution and contrast of the RPE: 1) changing the focus of the illumination while keeping the imaging channel focused on the RPE; 2) filter the detected light with a linear polarizer placed in the detector's pupil plane; and 3) use different wavelengths for illumination (680 and 790 nm).

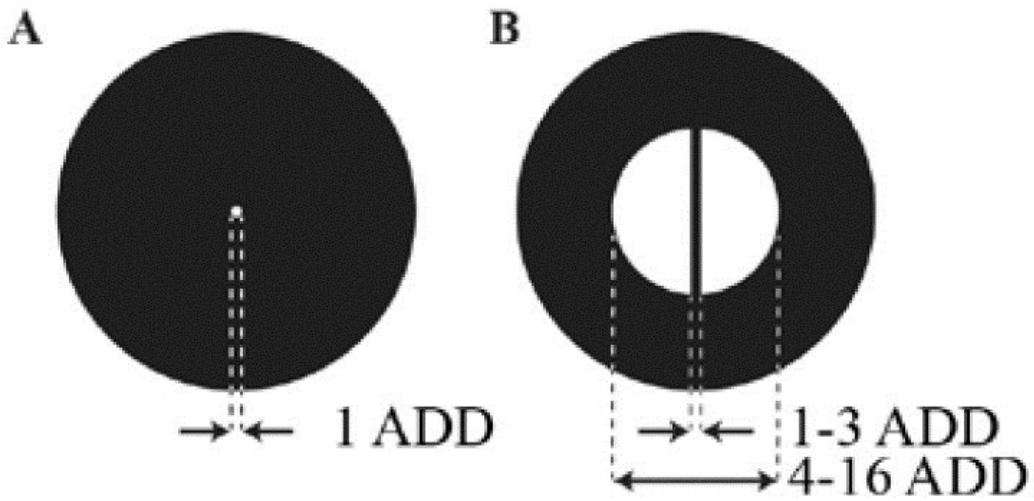

Fig. 1 AOSLO image plane apertures in front of the detector: a) traditional confocal pinhole, approximately one Airy disk diameter (ADD), and b) large pinhole with centered filament.

The imaging light sources were either a 790 nm super-luminescent diode (Superlum, Carrigtwohill, Co. Cork, Ireland) or a super-continuum light source (NKT photonics, Denmark) with a tunable band-pass filter (NKT Photonics, Birkerød, Denmark) centered either at 565 or 680 nm, with a 10 nm bandwidth. The wavefront sensing source was an 850 nm super-luminescent diode (Superlum). Incident powers for these light sources were 70, 60 and 17 μW respectively, measured at the cornea. The combined light exposure of all three sources was kept a minimum of 5 times below the maximum permissible exposure set forth by the ANSI Z136.1 [17,18]. Image sequences of 150 frames were collected and processed to remove the warp due to the sinusoidal motion of the horizontal scanner. Those images were then registered, and the 50 images with highest normalized cross-correlation relative to a user-selected reference frame were averaged to improve signal-to-noise ratio [32].

Image sequences were collected at the center of the macula and 10° visual angle lateral (temporal) to fixation using either a 1.00 or 1.75° square field of view. These locations were chosen to represent cone and rod dominated areas, respectively. First, confocal images of the photoreceptor layer (PRL) were collected, using a 1 ADD pinhole and no filament. This was followed by collection of dark-field image sequences at the same retinal location at multiple foci using various

pinholes and/or filaments. The time required to exchange and center apertures and filaments was approximately five minutes.

One of the most abundant features in the dark-field RPE images is bright spots which could be confused with photoreceptors. In order to study the relative position of these spots in the dark-field images relative to those of photoreceptors in confocal images, a 45:55% splitting ratio pellicle beam splitter (Thorlabs Inc., Newton, NJ, USA) was used during one imaging session to simultaneously record confocal and dark-field images in perfect registration. Both signals were collected using Hamamatsu H7422-50 photomultiplier modules (Hamamatsu Corporation, Bridgewater, NJ, USA).

2.4 AOSLO autofluorescence imaging

The visible channel of the AOSLO was used in subject AD_1025 to record visible RPE (lipofuscin) autofluorescence images in order to validate the dark-field RPE images. The lipofuscin autofluorescence was excited with the supercontinuum light source with the tunable filter reconfigured to provide 60 μW of corneal incident power at 565±5 nm for excitation. The resulting emission was collected using an interferometric optical filter with central wavelength 625 nm and 90 nm bandwidth. As in Morgan *et al.*'s work [16] high signal-to-noise ratio 790 nm confocal reflectance images were simultaneously recorded to create registered averages of the fluorescence images. The images were collected using a square 2.0° field of view, resulting in a light exposure at a level approximately 350 times below the ANSI Z136.1 maximum permissible exposure [17,18].

2.5 Image analysis

The photoreceptor and RPE mosaic images were analyzed in two ways. First, the radial average of the power spectrum was calculated for all images, with local maxima indicating the spatial frequency that corresponds to cell spacing [33]. Next a subset of the images were chosen for semi-automatic cell identification using custom Matlab software (The Mathworks Inc, Natick, MA, USA) based on the algorithm of Li and Roorda [34]. The cell coordinates were also used to

create Voronoi cell maps [35] and to estimate nearest neighbor distances.

2.6 Point spread function imaging

In order to measure the spatial extent of the dark-field and confocal signals, the point spread function (PSF) of subject JC_0616 was imaged near fixation using a Qicam camera (Qimaging, Surrey, BC, Canada) focused on the confocal aperture plane. The *in vivo* PSFs were recorded at the best focus for dark-field RPE with an exposure equivalent to one AOSLO frame (62.5 ms). After acquisition, 10 PSFs were averaged without registration.

3. Results

3.1 Dark-field RPE images

The dark-field aperture blocks the confocal signal from the retinal layer that is in focus. When focused onto the photoreceptors layer (inner/outer segment), this results in a dramatic attenuation of their signal, thus revealing the RPE mosaic behind, as illustrated in Fig. 2 and Fig. 3 . The panels in these figures show the photoreceptor mosaic as seen with confocal detection and the RPE seen with dark-field detection at the center of the macula (fixation) and 10° temporal to fixation. Similar to what is found in AOSLO autofluorescence images the RPE cells appear bright at the border and dark at their center. The best contrast in the RPE images was consistently obtained at the best confocal imaging focus for the photoreceptor mosaic for all volunteers, to within 0.025 diopters.

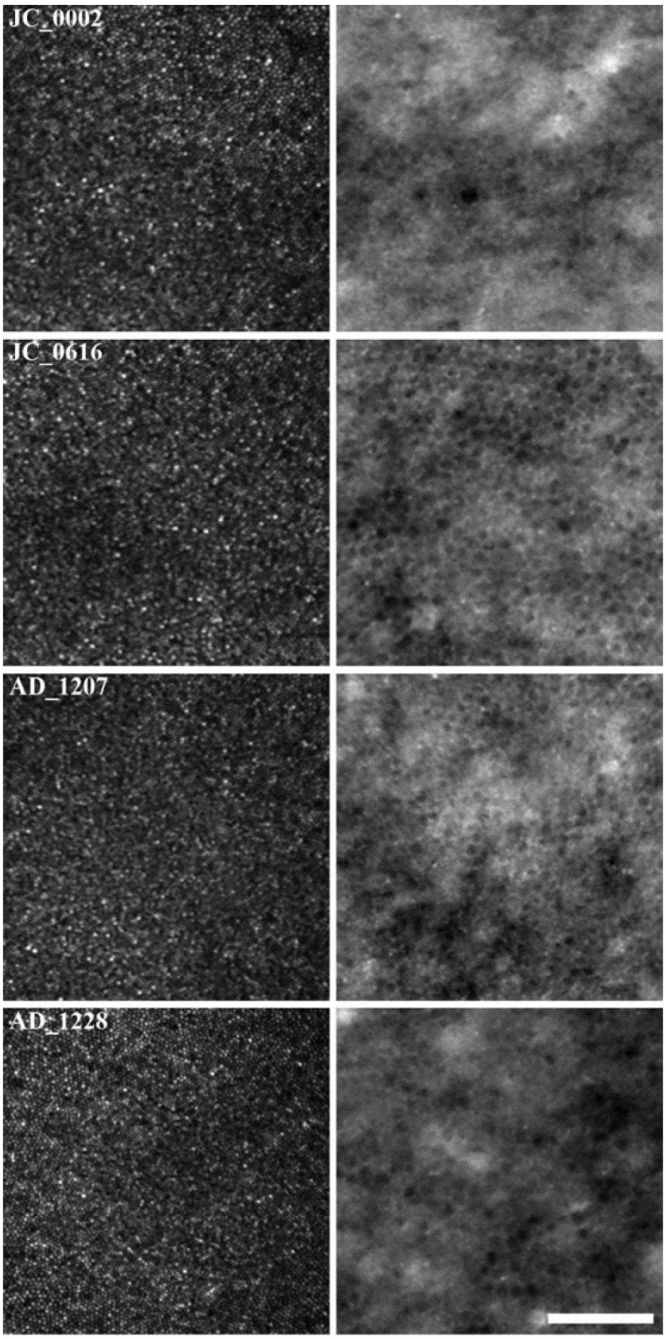

Fig. 2 AOSLO confocal (left) and dark-field (right) retinal images in four different subjects, all collected at the foveal center (center of fixation). The confocal images show the cone photoreceptor mosaic, while the dark-field images show the characteristic hexagonal RPE cell mosaic. The scale bar is 100 μm across.

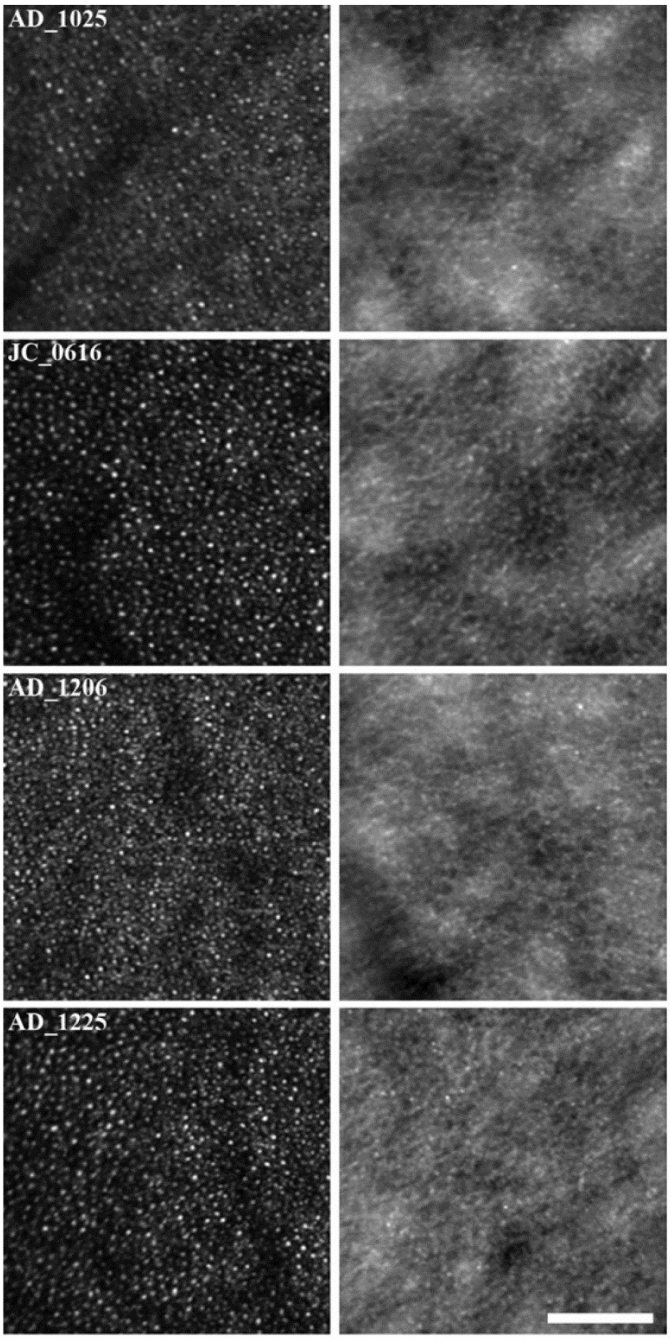

Fig. 3 AOSLO confocal (left) and dark-field (right) retinal images in four different subjects, all collected at 10° temporal to fixation. The confocal images show the cone and rod photoreceptor mosaic, while the dark-field images show the hexagonal RPE cell mosaic with significant cross-talk from the photoreceptor mosaic. The scale bar is 100 μm across.

All dark-field images show a mottled background consisting of dark and light patches many cell widths across. An *en face* view of the choroid at the same retinal location using a volume projection from a manually segmented SD-OCT data cube (shown in Fig. 4) shows reasonable correspondence with the pattern observed in the dark-field image. This supports the hypothesis that a significant fraction of the light captured by the detector in this technique has been reflected by the choroid, as proposed by Webb *et al.* [22].

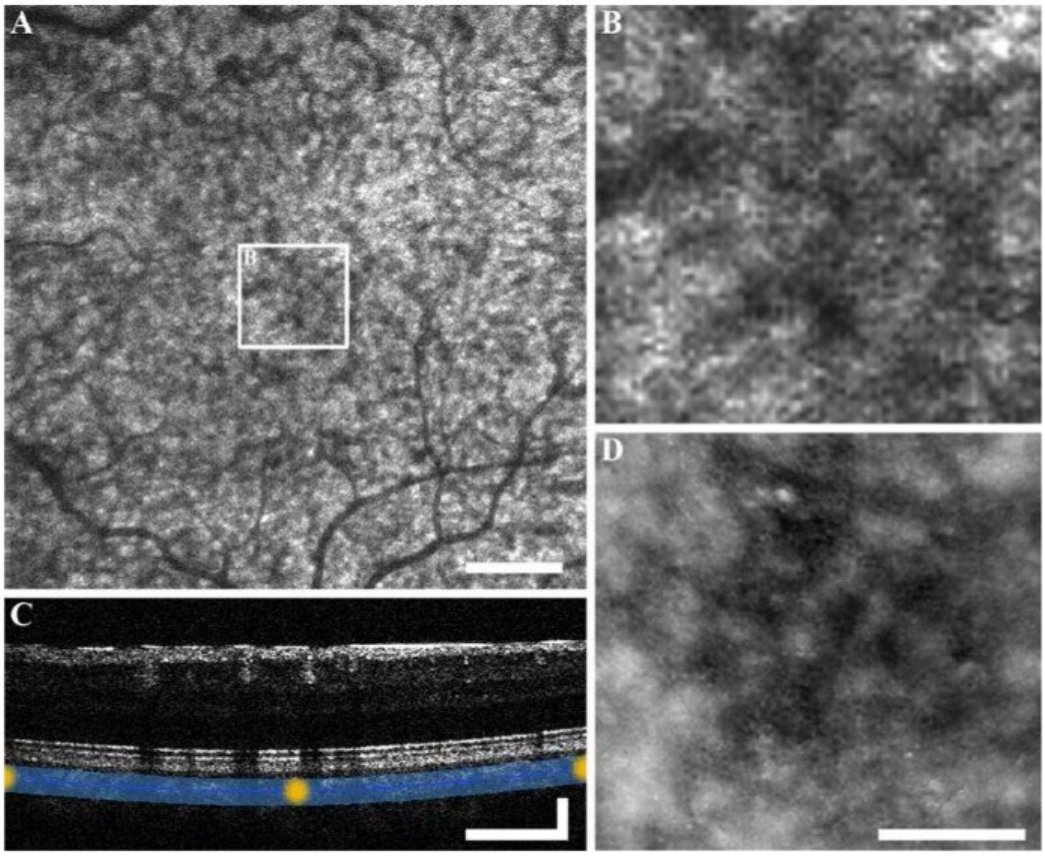

Fig. 4 Comparison of SD-OCT data and an AOSLO dark-field image (subject AD_1025). The *en face* view shown in B was created by coarsely segmenting the SD-OCT signal from the choroid over the area highlighted in panel A over the depth range indicated by the blue band. Panel D, shows the same retinal area as B as seen using AOSLO dark-field imaging. Scale bars are: A) 500 μm; C) 500 μm horizontal and 100 μm vertical; B) & D) 100 μm.

One of the most noticeable features in the AOSLO dark-field image presented in this work are the bright dots with sizes comparable to that of the rod and cone photoreceptors [36]. Confocal and dark-

field images were collected simultaneously and in perfect registration, in order to investigate the correspondence between the bright spots in both images (see Fig. 5). The resulting images indicate that not all bright dots in the RPE images correspond to a cone photoreceptor, instead the locations corresponding to cones could appear as both well-defined bright or dark spots. Automated identification of 5616 cones and comparison against the image intensity at the same locations in the RPE images show a poor cross-correlation coefficient (0.40).

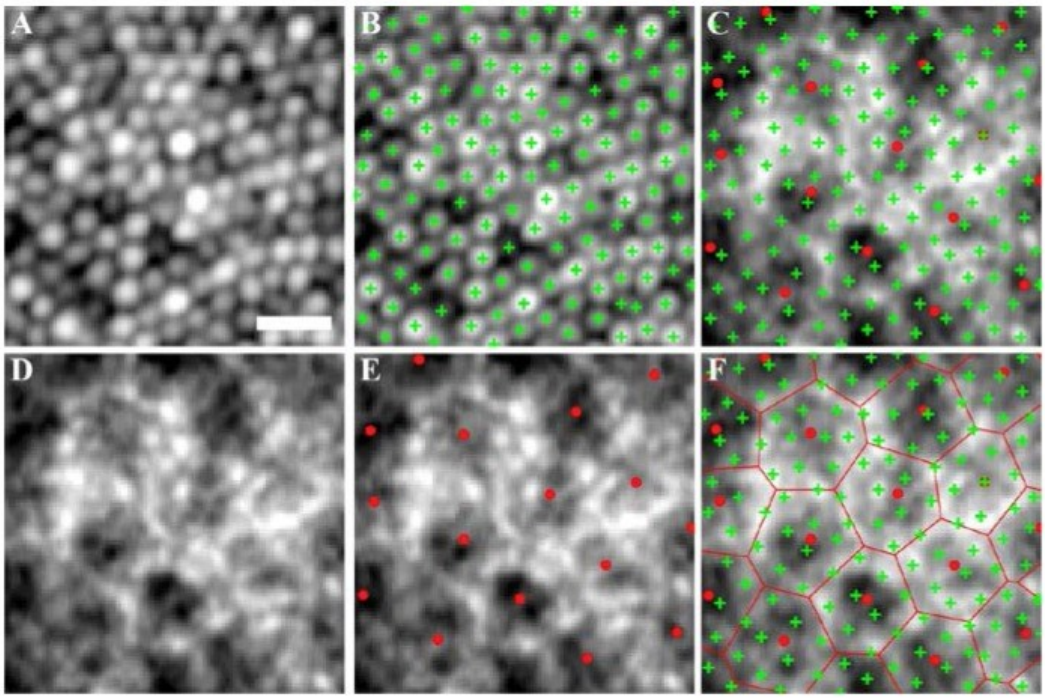

Fig. 5 Confocal (photoreceptor) and dark-field (RPE) images collected simultaneously (subject JC_0616) at approximately 0.8° from fixation. Panels A-B and C-F show cones recorded with 1 ADD pinhole and dark-field recorded with a 16 ADD pinhole and 1 ADD filament, respectively. Panels B and E show the cone and RPE cell centers marked with crosses and circles superimposed to the images in A and D, respectively. Panel C shows the dark-field image with cone centers and RPE centers superimposed, while panel F adds the cell borders, determined as Voronoi cells derived from the estimated cell centers. The scale bar is 10 μm across.

Most RPE cells could be manually identified at center of fixation in all volunteers (Fig. 2), while at 10° temporal to fixation this is a much harder task, and often not possible (Fig. 3). Although a full cell count could not be achieved with confidence in any of the images,

automatic estimation of cell spacing using the radial average of the image power spectrum showed good correspondence to manual measurements. The average nearest neighbor distance across all 7 subjects of 10.7±0.9 μm (± standard deviation) at the center of fixation, and 13.4±0.6 μm at 10° temporal to fixation, in good agreement with histologic [37] and *in vivo* studies [16]. A similar measurement derived from direct cone photoreceptor counting yielded 3.4±0.4 μm and 9.4±1.1 μm, respectively.

3.2 Dark-field filter obscuration and pinhole dimensions

In an attempt to attenuate the low spatial frequency pattern affecting the RPE dark-field images, 4, 8, 12 and 16 ADD diameter pinholes were tested by collecting images in the same subject at the same retinal location and focus. The resulting images (Fig. 6) show similar contrast and structures when using 8, 12 and 16 ADD pinholes. Images collected using a 4 ADD diameter pinhole, however, were consistently worse in that high spatial frequency structures make it more difficult to visualize the RPE mosaic.

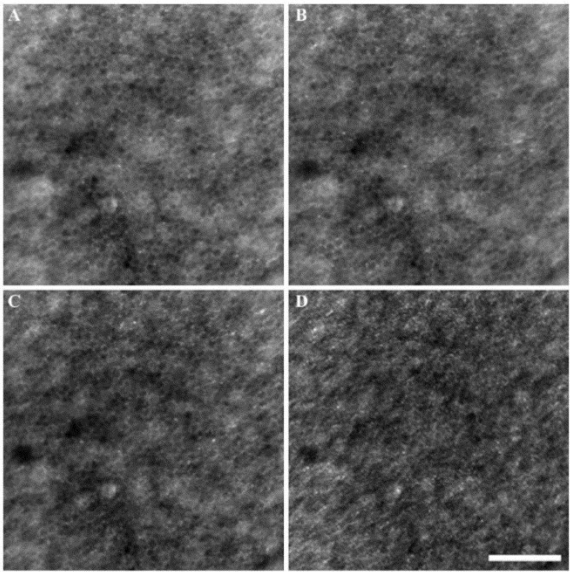

Fig. 6 Dark-field AOSLO images of the RPE mosaic at the center of fixation in volunteer JC_0616 collected using a 1 ADD thick filament and different pinhole diameters: A) 16, B) 12, C) 8 and D) 4 ADDs. The scale bar is 100 μm across.

The other key parameter of the dark-field filter is the diameter of the filament used to block the confocal signal. Comparison of dark-

field AOSLO images using a 1 and 3 ADD filament consistently showed that both filament widths provide comparable visualization of the RPE mosaic (see Fig. 7).

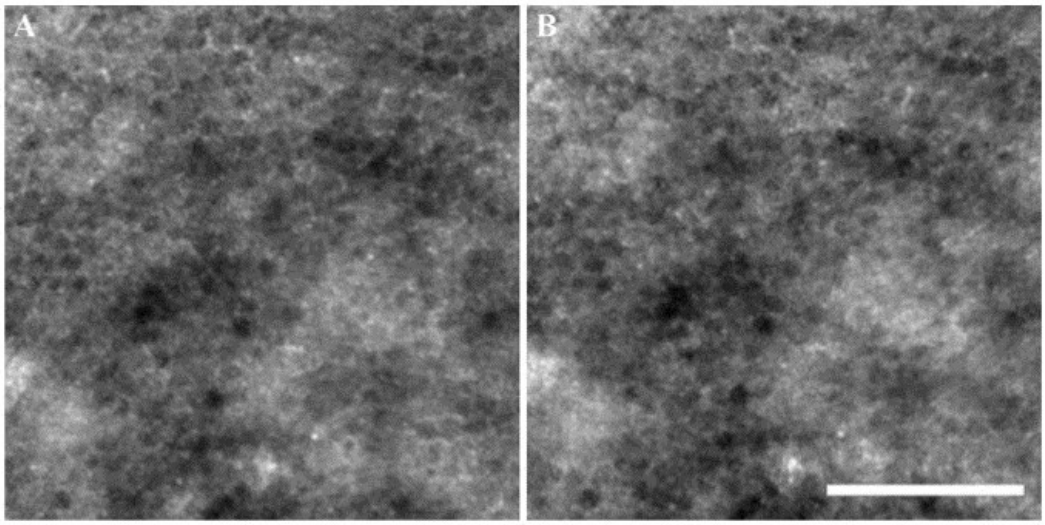

Fig. 7 Dark-field AOSLO images of the RPE mosaic at the center of fixation of volunteer JC_0616 collected using a 16 ADD diameter pinhole and either 1 (A) or 3 ADD thick filament (B). The scale bar is 100 μm across.

An additional experiment was performed to try to gain some understanding of the spatial extent of the RPE dark-field signal, by recording long exposure PSF images at the AOSLO detector's image plane (subject JC_0616). Fig. 8 shows one of those images, the radial average and the radial sum (integrated along the azimuthal coordinate). These curves are compared against a diffraction-limited PSF assuming a single, infinitesimally thin retinal reflecting layer. This is not the case in practice, even at the foveal center where the reflection from the nerve fiber layer is negligible relative to contributions of the photoreceptor and RPE layers. Therefore, due to the at least two distinct reflective layers (photoreceptors and RPE) a wider-than-theoretical PSF should be expected, as the PSFs originating at each layer are slightly defocused relative to each other. The experimental PSFs, collected at the foveal center (fixation) show, as expected, a significant portion of the energy outside the extent of the central lobe of the theoretical PSF (Airy disk). Interestingly, there are no obvious boundaries indicating the extent of the confocal or the dark-field RPE signals, neither in the radial average, nor in the radial sum of the experimental PSF.

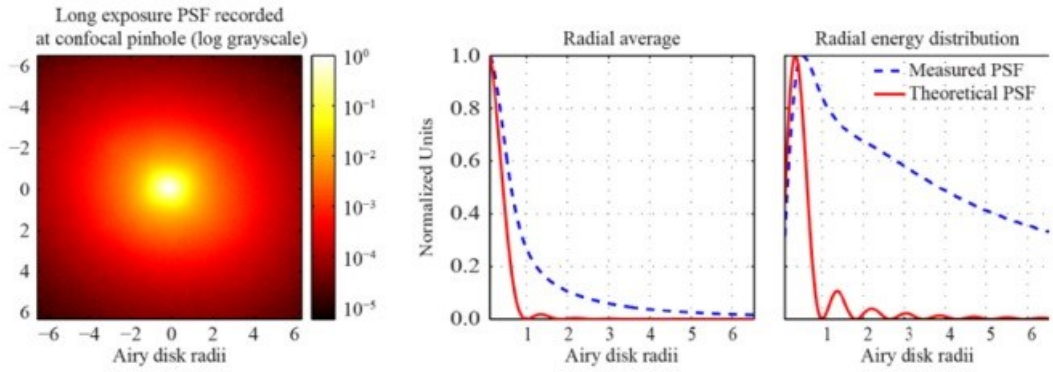

Fig. 8 Time-averaged retinal point-spread function (PSF) recorded from research volunteer JC_0616 (left), focused on the photoreceptor layer (logarithmic color scale). The central and right panels show the radial average and integral, respectively, compared to that of a single retinal layer theoretical PSF (red solid lines).

3.3 Dark-field imaging with visible and near infrared light

RPE images were collected at multiple retinal locations using 680 and 790 nm light to investigate the effect of wavelength on AOSLO dark-field contrast. The 680 nm images appear slightly blurrier, with the low spatial frequency choroidal features enhanced, as seen in Fig. 9 . Both these factors make the identification of individual RPE more difficult when imaging with the shorter wavelength.

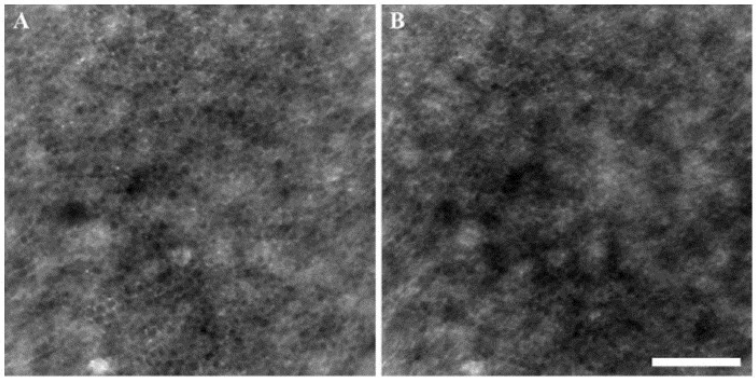

Fig. 9 Dark-field AOSLO images of the RPE mosaic at the center of fixation of volunteer JC_0616, using a 16 ADD diameter pinhole, 1 ADD thick filament and 790 nm (A) and 680nm (B) light. The scale bar is 100 μm across.

3.4 Apodization of entrance and/or exit pupils

In an attempt to further attenuate the cone photoreceptor reflectance signal in the dark-field images, a centered 3 mm diameter circular block was used in either the illumination or detection pupil planes [30]. The resulting images, shown in Fig. 10 , show that apodization of the imaging pupil produced a comparable image, which was slightly grainier due to the lower signal. Apodization of the illumination pupil, on the other hand, completely degraded the view of the RPE mosaic.

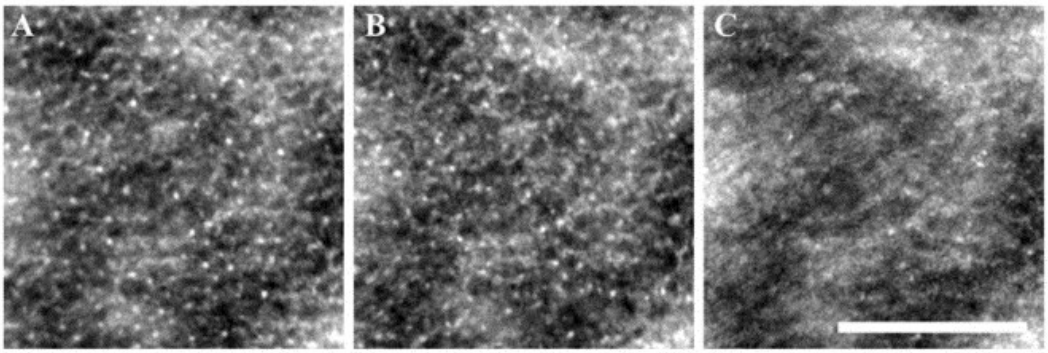

Fig. 10 Effect of pupil apodization on image quality and contrast at 10° temporal to fixation in volunteer JC_0616 using 790 nm illumination, 16 ADD pinhole, 1 ADD filament (A) and with a centered 3 mm diameter circular block in the imaging (B) or the illumination paths (C). The scale bar is 100 μm across.

3.5 Validation of AOSLO dark-field RPE images

The AOSLO dark-field RPE imaging was validated using RPE autofluorescence AOSLO imaging. Images were recorded at the same retinal locations with both techniques in a subject with no eye disease. Ignoring the low spatial frequency structures from the choroid and the shadows of the retinal vasculature, both techniques show the edges of the RPE cells as brighter than the center (see Fig. 11). This might suggest that the scattering source is colocalized with the lipofuscin granules.

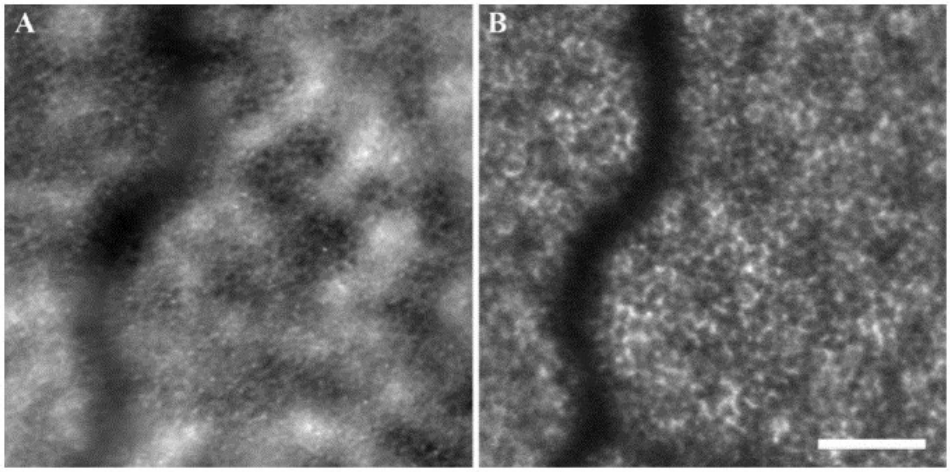

Fig. 11 Comparison of autofluorescence to dark-field RPE imaging in AD_1025 at 3° superior and 9° temporal from fixation. A) dark-field image, B) autofluorescence images collected using 565 nm excitation and 625±45 nm emission. The scale bar is 100 μm across.

We sought further validation of the RPE dark-field images by collecting AOSLO reflectance and dark-field images in one patient diagnosed with central serous retinopathy. In this condition, the retina detaches from the RPE at some locations, thus providing a direct view of the RPE mosaic without interference from the photoreceptor layer, when imaging with a confocal AOSLO [21]. Images of the same retinal location show good correspondence between AOSLO dark-field and confocal imaging where the photoreceptor layer is clearly displaced from the RPE (Fig. 12).

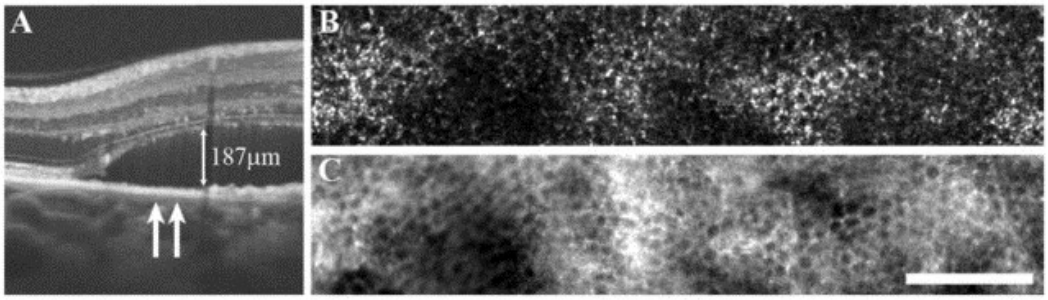

Fig. 12 RPE images collected in a patient DW_1188 with central serous retinopathy. The SD-OCT image in panel A shows the 187 μm thick fluid collection that separates the retina from the RPE (below). *En face* AOSLO images of the area between the white arrows in A show RPE morphology in confocal mode (B), as well as in dark-field mode (C) at this location approximately 6° superior to fixation. The scale bar is 100 μm across.

4. Discussion

The modification of an AOSLO detection path by blocking the confocal signal and collecting what has been referred to as the indirect or dark-field signal, shows a dramatic attenuation of the light back-scattered by the photoreceptor inner and outer segments, thus revealing the RPE mosaic. It appears that a large proportion of the light that reaches the detector in this configuration has been multiply scattered and reached as deep as the choroid. Furthermore, the good correspondence between SD-OCT and dark-field AOSLO low spatial frequency intensity profiles suggests that the choroid might be critical for the visualization of the RPE using dark-field and that this technique can be also thought of as retro-illumination. The poorer visualization of the RPE mosaic when using 680 nm light when compared with 790 nm, is consistent with the lower retinal and choroidal penetration of shorter wavelengths [23].

Dark-field imaging with different pinhole diameter and filament thickness, as well as PSF imaging, showed that there are no clear optimal dimensions for the dark-field mask in terms of RPE visualization. Loosely, it appears that the central block should be equal or larger than one Airy disk in diameter and the pinhole larger than 4 Airy disks in diameter. This is consistent with the idea that dark-field imaging requires blocking the reflected or single-scattered light that would be found in the central Airy disk.

Although we have shown that visualizing the RPE mosaic is possible using the proposed technique, identification of individual RPE cells is not always possible. In fact, additional point-like structures, potentially due to residual photoreceptor signal make cell identification very difficult in the rod-dominated areas outside the macula. Two additional experiments (data not shown) were performed in an attempt to further attenuate any potential non-confocal light back-scattered by the photoreceptors. First, we defocused the illumination source, hoping to reduce the coupling of light onto the photoreceptor inner/outer segments, as we intended when using the annular pupil masks mentioned above. Second, a linear polarizer was placed in the pupil plane of the detector plane, and images where collected at 10° temporal to fixation at the orientations that produce dark-field RPE

images with maximum intensity, then at 45 and 90° relative to it. Neither approach improved the contrast of the RPE mosaic.

The RPE images recorded with dark-field AOSLO have generally lower contrast than those acquired using autofluorescence collected both in this (Fig. 11) and previous work [15,16]. Dark-field imaging seems to reveal RPE structure, although further investigation on the nature of the bright dots that form these images is required, before this modality can be adopted for screening and/or diagnosing eye disease. Despite showing poorer contrast than autofluorescence, dark-field RPE imaging is an appealing avenue for studying eye disease at the microscopic scale non-invasively. When compared to AOSLO autofluorescence imaging, dark-field AOSLO imaging requires one less light source and imaging channel [15,16], less complex data processing and provides increased patient comfort and light safety with no concerns about potential photochemical damage. It still remains to be studied in healthy and diseased eyes whether these two techniques provide identical or complementary information.

5. Conclusions

AOSLO dark-field has been demonstrated for imaging of the RPE cell mosaic non-invasively in human subjects. The implementation of this technique requires minimal modification of existing and future AOSLOs, namely replacing the confocal aperture by a larger one with a central obscuration to block the confocal signal. In this study, due to cost and availability, we implemented a filament of known thickness, although a circular obscuration would have been preferable in terms of signal strength and symmetry.

For reasons not yet fully understood, the images from the foveal center, an area dominated by cone photoreceptors, provide a clearer view of the RPE cell boundaries, with nearly all cells visible in some volunteers, as shown in Fig. 13 . Multiple parameters were explored to try to improve the visualization of the RPE cell boundaries including: pinhole diameter, obscuration filament thickness, illumination and imaging pupil apodization, unmatched imaging and illumination focus, wavelength and polarization. None of these offered a clear benefit and some even lead to poorer RPE visualization.

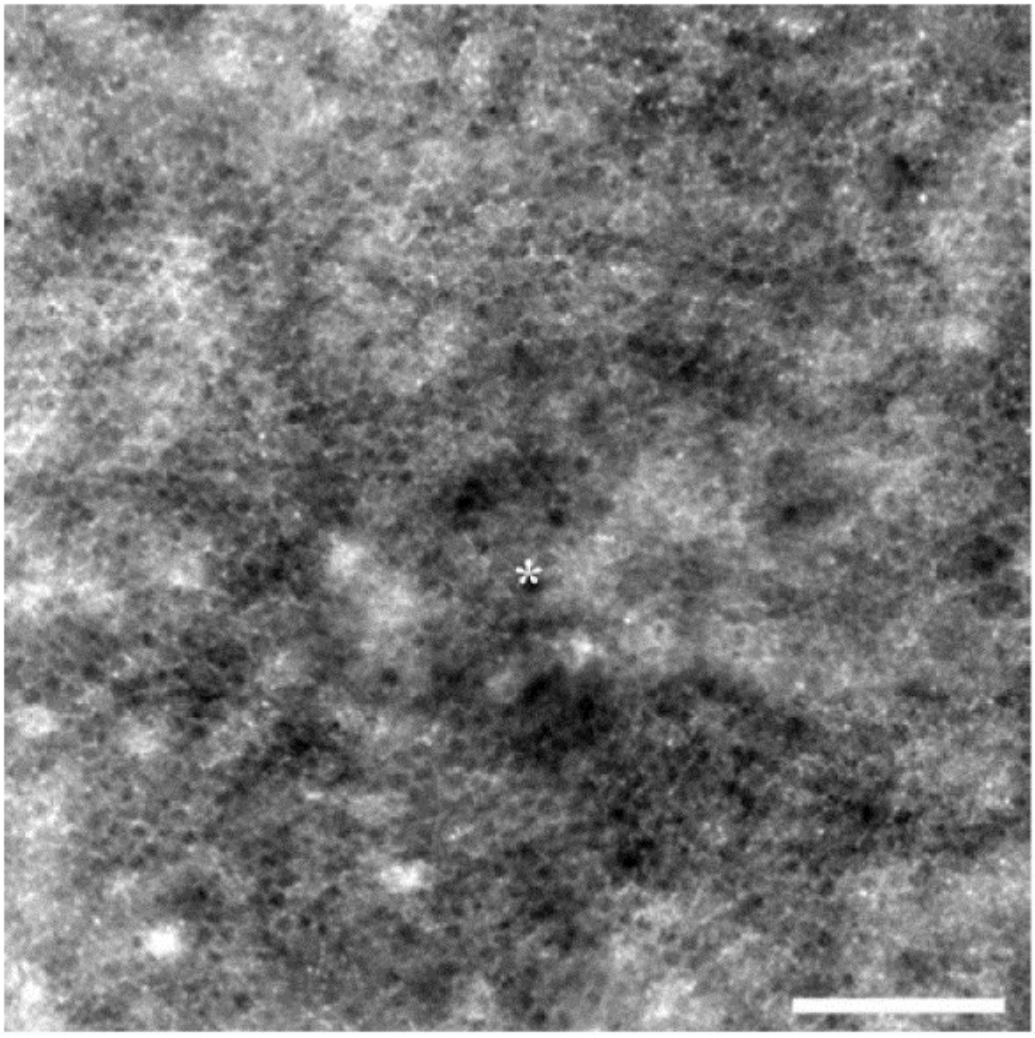

Fig. 13 AOSLO dark-field view from the fovea of volunteer JC_0616, with '*' denoting the point of maximum cone density. The scale bar is 100 μm across.

Dark-field AOSLO could be a useful tool in the study of retinal disease mechanisms. In particular, in macular degeneration, RPE cells often change morphology before widespread degeneration and atrophy [4]. This technique could also be translated into a clinical tool for screening, monitoring progression of disease, and evaluation of therapeutic interventions.

Acknowledgments

We would like to acknowledge the help of Chris Langlo in the preparation of this manuscript and Robert Cooper for the use of his

OCT alignment and averaging software. Funding: NIH grants P30EY001931, UL1RR031973 and T32GM07356. Alfredo Dubra-Suarez is the recipient of a Career Development Award from Research to Prevent Blindness (RPB) and a Career Award at the Scientific Interface from the Burroughs Wellcome Fund. This research was also supported by grants from the RD & Linda Peters Foundation and an unrestricted departmental grant from RPB. This investigation was conducted in a facility constructed with support from the Research Facilities Improvement Program; grant number C06-RR016511 from the National Center for Research Resources, NIH.

References

1. Spitznas M., Hogan M. J., "Outer segments of photoreceptors and the retinal pigment epithelium. Interrelationship in the human eye," Arch. Ophthalmol. 84(6), 810–819 (1970).10.1001/archopht.1970.00990040812022
2. Bok D., "Retinal photoreceptor-pigment epithelium interactions. Friedenwald lecture," Invest. Ophthalmol. Vis. Sci. 26(12), 1659–1694 (1985).
3. Steinberg R. H., "Interactions between the retinal pigment epithelium and the neural retina," Doc. Ophthalmol. 60(4), 327–346 (1985).10.1007/BF00158922
4. Ambati J., Fowler B. J., "Mechanisms of age-related macular degeneration," Neuron 75(1), 26–39 (2012).10.1016/j.neuron.2012.06.018
5. Simó R., Villarroel M., Corraliza L., Hernández C., Garcia-Ramírez M., "The retinal pigment epithelium: something more than a constituent of the blood-retinal barrier--implications for the pathogenesis of diabetic retinopathy," J. Biomed. Biotechnol. 2010, 190724 (2010).10.1155/2010/190724
6. Glazer L. C., Dryja T. P., "Understanding the etiology of Stargardt's disease," Ophthalmol. Clin. North. Am. 15, 93-100 (2002).
7. Blodi C. F., Stone E. M., "Best's vitelliform dystrophy," Ophthalmic Paediatr. Genet. 11(1), 49–59 (1990).
8. Marlhens F., Bareil C., Griffoin J. M., Zrenner E., Amalric P., Eliaou C., Liu S. Y., Harris E., Redmond T. M., Arnaud B., Claustres M., Hamel C. P., "Mutations in RPE65 cause Leber's congenital amaurosis," Nat. Genet. 17(2), 139–141 (1997).10.1038/ng1097-139
9. Greenstein V. C., Duncker T., Holopigian K., Carr R. E., Greenberg J. P., Tsang S. H., Hood D. C., "Structural and functional changes associated with normal and abnormal fundus autofluorescence in patients with

retinitis pigmentosa," Retina 32(2), 349–357 (2012).10.1097/IAE.0b013e31821dfc17
10. Schmitz-Valckenberg S., Holz F. G., Bird A. C., Spaide R. F., "Fundus autofluorescence imaging: review and perspectives," Retina 28(3), 385–409 (2008).10.1097/IAE.0b013e318164a907
11. Kellner U., Kellner S., Weber B. H., Fiebig B., Weinitz S., Ruether K., "Lipofuscin- and melanin-related fundus autofluorescence visualize different retinal pigment epithelial alterations in patients with retinitis pigmentosa," Eye (Lond.) 23(6), 1349–1359 (2009).10.1038/eye.2008.280
12. Kellner U., Kellner S., Weinitz S., "Fundus autofluorescence (488 NM) and near-infrared autofluorescence (787 NM) visualize different retinal pigment epithelium alterations in patients with age-related macular degeneration," Retina 30(1), 6–15 (2010).10.1097/IAE.0b013e3181b8348b
13. Spaide R. F., Curcio C. A., "Anatomical correlates to the bands seen in the outer retina by optical coherence tomography: literature review and model," Retina 31(8), 1609–1619 (2011).10.1097/IAE.0b013e3182247535
14. Fleckenstein M., Charbel Issa P., Helb H. M., Schmitz-Valckenberg S., Finger R. P., Scholl H. P., Loeffler K. U., Holz F. G., "High-resolution spectral domain-OCT imaging in geographic atrophy associated with age-related macular degeneration," Invest. Ophthalmol. Vis. Sci. 49(9), 4137–4144 (2008).10.1167/iovs.08-1967
15. Gray D. C., Merigan W., Wolfing J. I., Gee B. P., Porter J., Dubra A., Twietmeyer T. H., Ahamd K., Tumbar R., Reinholz F., Williams D. R., "In vivo fluorescence imaging of primate retinal ganglion cells and retinal pigment epithelial cells," Opt. Express 14(16), 7144–7158 (2006).10.1364/OE.14.007144
16. Morgan J. I., Dubra A., Wolfe R., Merigan W. H., Williams D. R., "In vivo autofluorescence imaging of the human and macaque retinal pigment epithelial cell mosaic," Invest. Ophthalmol. Vis. Sci. 50(3), 1350–1359 (2008).10.1167/iovs.08-2618
17. ANSI, "American National Standard for Safe Use of Lasers in Research, Development, or Testing," (Laser Institute of America, Orlando, FL, 2007).
18. Delori F. C., Webb R. H., Sliney D. H., American National Standards Institute , "Maximum permissible exposures for ocular safety (ANSI 2000), with emphasis on ophthalmic devices," J. Opt. Soc. Am. A 24(5), 1250–1265 (2007).10.1364/JOSAA.24.001250
19. Morgan J. I. W., Hunter J. J., Masella B., Wolfe R., Gray D. C., Merigan W. H., Delori F. C., Williams D. R., "Light-induced retinal changes observed with high-resolution autofluorescence imaging of the retinal

pigment epithelium," Invest. Ophthalmol. Vis. Sci. 49(8), 3715–3729 (2008).10.1167/iovs.07-1430

20. Cideciyan A. V., Jacobson S. G., Aleman T. S., Gu D., Pearce-Kelling S. E., Sumaroka A., Acland G. M., Aguirre G. D., "In vivo dynamics of retinal injury and repair in the rhodopsin mutant dog model of human retinitis pigmentosa," Proc. Natl. Acad. Sci. U.S.A. 102(14), 5233–5238 (2005).10.1073/pnas.0408892102
21. Roorda A., Zhang Y., Duncan J. L., "High-resolution in vivo imaging of the RPE mosaic in eyes with retinal disease," Invest. Ophthalmol. Vis. Sci. 48(5), 2297–2303 (2007).10.1167/iovs.06-1450
22. Webb R. H., Hughes G. W., Delori F. C., "Confocal scanning laser ophthalmoscope," Appl. Opt. 26(8), 1492–1499 (1987).10.1364/AO.26.001492
23. Elsner A. E., Burns S. A., Weiter J. J., Delori F. C., "Infrared imaging of sub-retinal structures in the human ocular fundus," Vision Res. 36(1), 191–205 (1996).10.1016/0042-6989(95)00100-E
24. Yoshida A., Ishiko S., Akiba J., Kitaya N., Nagaoka T., "Radiating retinal folds detected by scanning laser ophthalmoscopy using a diode laser in a dark-field mode in idiopathic macular holes," Graefes Arch. Clin. Exp. Ophthalmol. 236(6), 445–450 (1998).10.1007/s004170050104
25. Shin Y. U., Lee B. R., "Retro-mode Imaging for retinal pigment epithelium alterations in central serous chorioretinopathy," Am. J. Ophthalmol 154, 155–163 (2012).
26. Chui T. Y., Vannasdale D. A., Burns S. A., "The use of forward scatter to improve retinal vascular imaging with an adaptive optics scanning laser ophthalmoscope," Biomed. Opt. Express 3(10), 2537–2549 (2012).10.1364/BOE.3.002537
27. R. Wayne, *Light and Video Microscopy* (Academic Press/Elsevier, 2009).
28. Tanna H., Dubis A. M., Ayub N., Tait D. M., Rha J., Stepien K. E., Carroll J., "Retinal imaging using commercial broadband optical coherence tomography," Br. J. Ophthalmol. 94(3), 372–376 (2010).10.1136/bjo.2009.163501
29. Dubra A., Sulai Y., "Reflective afocal broadband adaptive optics scanning ophthalmoscope," Biomed. Opt. Express 2(6), 1757–1768 (2011).10.1364/BOE.2.001757
30. Sulai Y. N., Dubra A., "Adaptive optics scanning ophthalmoscopy with annular pupils," Biomed. Opt. Express 3(7), 1647–1661 (2012).10.1364/BOE.3.001647
31. Stiles W., Crawford B., "The luminous efficiency of rays entering the eye pupil at different points," Proc. R. Soc. Lond. B Biol. Sci. 112(778), 428–450 (1933).10.1098/rspb.1933.0020
32. A. Dubra and Z. Harvey, "Registration of 2D Images from Fast Scanning Ophthalmic Instruments," in *The 4th International Workshop on*

Biomedical Image Registration (Springer-Verlag, 2010), 60-71.10.1007/978-3-642-14366-3_6

33. Cooper R. F., Langlo C. S., Dubra A., Carroll J., "Automatic detection of modal spacing (Yellott's ring) in adaptive optics scanning light ophthalmoscope images," Ophthalmic Physiol. Opt. 33(4), 540–549 (2013).10.1111/opo.12070
34. Li K. Y., Roorda A., "Automated identification of cone photoreceptors in adaptive optics retinal images," J. Opt. Soc. Am. A 24(5), 1358–1363 (2007).10.1364/JOSAA.24.001358
35. Baraas R. C., Carroll J., Gunther K. L., Chung M., Williams D. R., Foster D. H., Neitz M., "Adaptive optics retinal imaging reveals S-cone dystrophy in tritan color-vision deficiency," J. Opt. Soc. Am. A 24(5), 1438–1447 (2007).10.1364/JOSAA.24.001438
36. Dubra A., Sulai Y., Norris J. L., Cooper R. F., Dubis A. M., Williams D. R., Carroll J., "Noninvasive imaging of the human rod photoreceptor mosaic using a confocal adaptive optics scanning ophthalmoscope," Biomed. Opt. Express 2(7), 1864–1876 (2011).10.1364/BOE.2.001864
37. Dorey C. K., Wu G., Ebenstein D., Garsd A., Weiter J. J., "Cell loss in the aging retina. Relationship to lipofuscin accumulation and macular degeneration," Invest. Ophthalmol. Vis. Sci. 30(8), 1691–1699 (1989).